Supplement of J. Micropalaeontol., 45, 1–25, 2026
https://doi.org/10.5194/jm-45-1-2026-supplement

Journal of Micropalaeontology
Open Access

Supplement of

Tropical ecosystem shifts at the Eocene–Oligocene transition in the southwestern Caribbean region

Raúl Trejos-Tamayo et al.

Correspondence to: Raúl Trejos-Tamayo (raul.trejos.tamayo@gmail.com)

This PDF file include the following:
Figures

Tables

References

Supplementry information

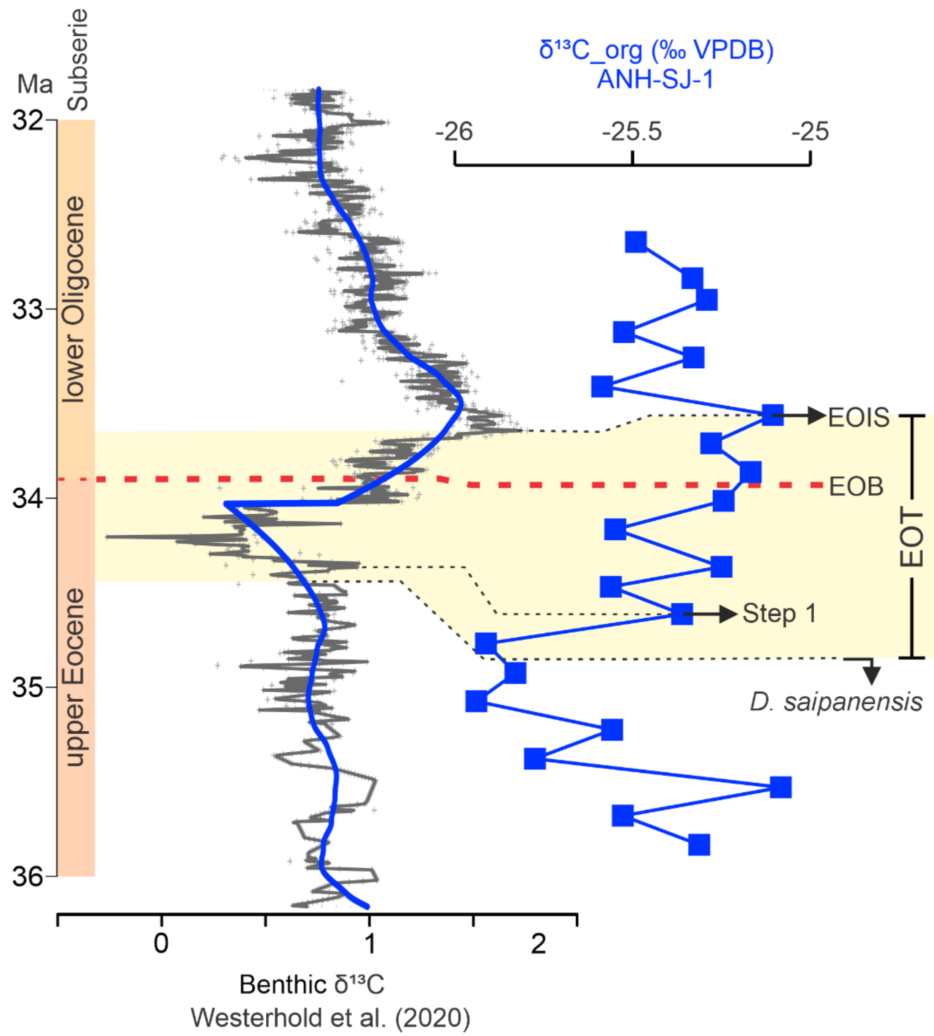

Figure S1. Comparison between the $\delta^{13}C$_org record from core ANH-SJ-1 (blue line and squares) and the global benthic $\delta^{13}C$ stack from Westerhold et al. (2020) (gray crosses and blue line). The red dashed line marks the EOB, and the shaded yellow band represents the broader EOT. Key events are highlighted, including the Earliest Oligocene Oxygen Isotope Step (EOIS) at ~33.7 Ma and Step 1 of the carbon isotope excursion at ~34.2 Ma, as per Hutchinson et al. (2021). The extinction level of *Discoaster saipanensis* is also shown. Chronostratigraphic subseries are indicated on the left. This correlation supports the placement of isotopic tie points used in the age model.

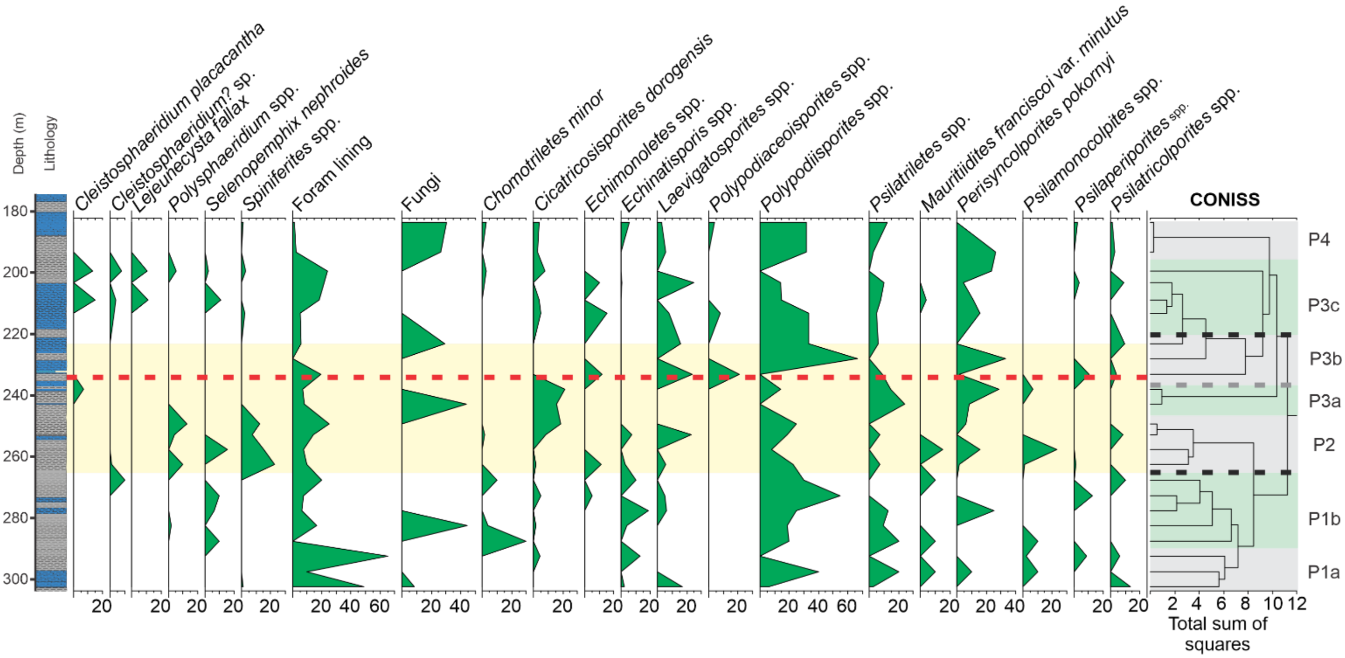

Figure S2. Distribution of the main palynomorph taxa (>5% relative abundance) across the upper Eocene–lower Oligocene interval in core ANH-SJ-1. The yellow shaded band represents the EOT, and the red dashed line indicates the position of the EOB, as defined by the age model developed in this study. The dendrogram on the right shows the results of the CONISS cluster analysis based on palynological assemblages. Cluster groups P1a–P4, labeled on the dendrogram, reflect stratigraphically constrained ecological zones. Notably, the transition from group P1b to P2 aligns with the onset of the EOT, while the shift from P3b to P3c marks the end of the transition. These assemblage boundaries correspond closely with the chronostratigraphic framework, supporting the paleoenvironmental significance of the subdivision.

Table S5. Temperature affinities for selected calcareous nannofossils species analyzed in this study, as proposed by different authors.

Temperature	Species	Authors	Observation
Cold	*Chiasmolithus altus*	Bukry (1973), Wei and Wise (1990), Villa et al. (2014)	
	Chiasmolithus spp.	Bukry (1973), Wei and Wise (1990), Villa et al. (2014)	
Temperate	*Coccolithus eopelagicus*	Villa et al. (2008)	
	Coccolithus pelagicus	Persico and Villa (2004), Villa et al. (2008)	
	Cyclicargolithus floridanus	Wei and Wise (1990)	
	Reticulofenestra bisecta	Villa et al. (2014)	Cold in Villa et al. (2008)
	Reticulofenestra dictyoda	Cappelli et al. (2019)	
	Reticulofenestra erbae	Cappelli et al. (2019)	
	Reticulofenestra isabellae	Cappelli et al. (2019)	
	Reticulofenestra lockeri	Cappelli et al. (2019)	
	Reticulofenestra lockeri gr.	Cappelli et al. (2019)	
	Reticulofenestra perplexa	Cappelli et al. (2019)	
	Reticulofenestra reticulata	Cappelli et al. (2019)	
	Reticulofenestra stavensis	Cappelli et al. (2019)	
	Reticulofenestra umbilicus	Villa et al. (2014)	
	Reticulofenestra spp.	Cappelli et al. (2019)	
	Toweius callosus	Cappelli et al. (2019)	
Warm	*Coccolithus formosus*	Wei and Wise (1990), Tremolada and Bralower (2004), Villa et al. (2014). Cappelli et al. (2019)	
	Discoaster barbadiensis	Wei and Wise (1990), Tremolada and Bralower (2004), Villa et al. (2014), Cappelli et al. (2019)	
	Discoaster deflandrei	Wei and Wise (1990), Tremolada and Bralower (2004), Villa et al. (2014), Cappelli et al. (2019)	
	Discoaster saipanensis	Wei and Wise (1990), Tremolada and Bralower (2004), Villa et al. (2014), Cappelli et al. (2019)	
	Discoaster spp.	Wei and Wise (1990), Tremolada and Bralower (2004), Villa et al. (2014), Cappelli et al. (2019)	
	Helicosphaera compacta	Wei and Wise (1990)	
	Helicosphaera reticulata	Wei and Wise (1990)	
	Helicosphaera cf. *euphratis*	Wei and Wise (1990)	
	Helicosphaera euphratis	Wei and Wise (1990)	
	Helicosphaera spp.	Wei and Wise (1990)	

Helicosphaeroides intermedia	Wei and Wise (1990)	
Isthmolithus recurvus	Cappelli et al. (2019)	Temperate in Villa et al. (2014)
Sphenolithus cf. *radians*	Aubry (1992), Cappelli et al. (2019)	
Sphenolithus akropodus	Cappelli et al. (2019)	
Sphenolithus cf. *distentus*	Cappelli et al. (2019)	
Sphenolithus moriformis	Cappelli et al. (2019)	
Sphenolithus peartiae	Cappelli et al. (2019)	
Sphenolithus predistentus	Cappelli et al. (2019)	
Sphenolithus spp.	Cappelli et al. (2019)	
Zygrhabilithus bijugatus	Cappelli et al. (2019)	Cold in Agnini et al. (2007)

Table S6. Trophic affinities for selected calcareous nannofossils species analyzed in this study, as proposed by different authors.

Trophism	Species	Authors	Observations
Eutrophic	*Braarudosphaera bigelowii*	Siesser et al. (1992), Vieyra-Mexicano et al. (2024); Cao et al., 2024	
	Clausicoccus subdistichus	Wei and Wise (1990), Newsam et al. (2017)	
	Cyclicargolithus floridanus	Aubry (1992)	
	Chiasmolithus altus	Monechi et al. (2000)	
	Chiasmolithus spp.	Villa et al. (2014)	
	Isthmolithus recurvus	Villa et al. (2014)	
	Reticulofenestra umbilicus	Villa et al. (2014)	
	Helicosphaera compacta	Ziveri et al. (1995), Ziveri et al. (2004)	
	Helicosphaera reticulata	Ziveri et al. (1995), Ziveri et al. (2004)	
	Helicosphaera cf. *euphratis*	Ziveri et al. (1995), Ziveri et al. (2004)	
	Helicosphaera euphratis	Ziveri et al. (1995), Ziveri et al. (2004)	
	Helicosphaera spp.	Ziveri et al. (1995), Ziveri et al. (2004)	
	Helicosphaeroides intermedia	Ziveri et al. (1995), Ziveri et al. (2004)	
Mesotrophic	*Reticulofenestra dictyoda*	Cappelli et al. (2019)	
	Reticulofenestra erbae	Cappelli et al. (2019)	
	Reticulofenestra isabellae	Cappelli et al. (2019)	
	Reticulofenestra lockeri	Cappelli et al. (2019)	
	Reticulofenestra lockeri gr.	Cappelli et al. (2019)	
	Reticulofenestra perplexa	Cappelli et al. (2019)	
	Reticulofenestra stavensis	Cappelli et al. (2019)	
	Reticulofenestra spp.	Cappelli et al. (2019)	
	Toweius callosus	Cappelli et al. (2019)	
	Reticulofenestra bisecta	Cappelli et al. (2019)	
Oligotrophic	*Coccolithus formosus*	Tremolada and Bralower (2004), Villa et al. (2008), Cappelli et al. (2019)	
	Reticulofenestra reticulata	Aubry (1992), Tremolada and Bralower (2004) Villa et al. (2014), Cappelli et al. (2019)	
	Discoaster barbadiensis	Aubry (1992), Tremolada and Bralower (2004) Villa et al. (2014), Cappelli et al. (2019)	
	Discoaster deflandrei	Aubry (1992), Tremolada and Bralower (2004). Villa et al. (2014), Cappelli et al. (2019)	
	Discoaster saipanensis	Aubry (1992), Tremolada and Bralower (2004). Villa et al. (2014), Cappelli et al. (2019)	
	Discoaster spp.	Aubry (1992), Tremolada and Bralower (2004) Villa et al. (2014), Cappelli et al. (2019)	
	Sphenolithus cf. *radians*	Villa et al. (2014)	
	Sphenolithus akropodus	Villa et al. (2014)	

Sphenolithus cf. *distentus*	Villa et al. (2014)	
Sphenolithus moriformis	Villa et al. (2014)	
Sphenolithus peartiae	Villa et al. (2014)	
Sphenolithus predistentus	Villa et al. (2014)	
Sphenolithus spp.	Villa et al. (2014)	
Umbolicosphaera spp.	Villa et al. (2014)	
Zygrhabilithus bijugatus	Cappelli et al. (2019)	
Coccolithus pelagicus	Cappelli et al. (2019)	Eutrophic. Villa et al. (2014)

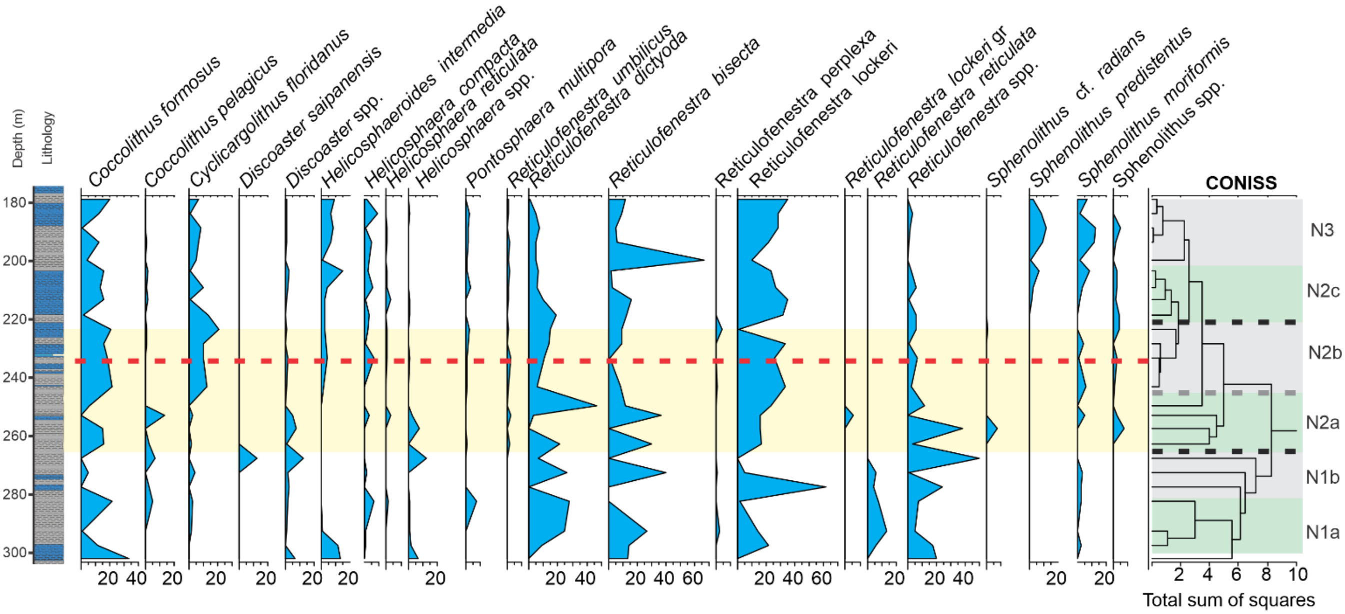

Figure S3. Distribution of the main calcareous nannofossil taxa (>5% relative abundance) across the upper Eocene–lower Oligocene interval in core ANH-SJ-1. The yellow shaded band represents the EOT, and the red dashed line marks the position of the EOB, as constrained by the age model developed in this study. The dendrogram on the right shows the results of the CONISS cluster analysis based on nannofossil assemblages. Cluster groups N1a–N3, labeled on the dendrogram, define stratigraphically constrained ecological zones. The transition from group N1b to N2a aligns closely with the onset of the EOT, while the shift from N2b to N2c corresponds to its termination. These shifts provide additional ecological support for the chronostratigraphic subdivisions used in this study.

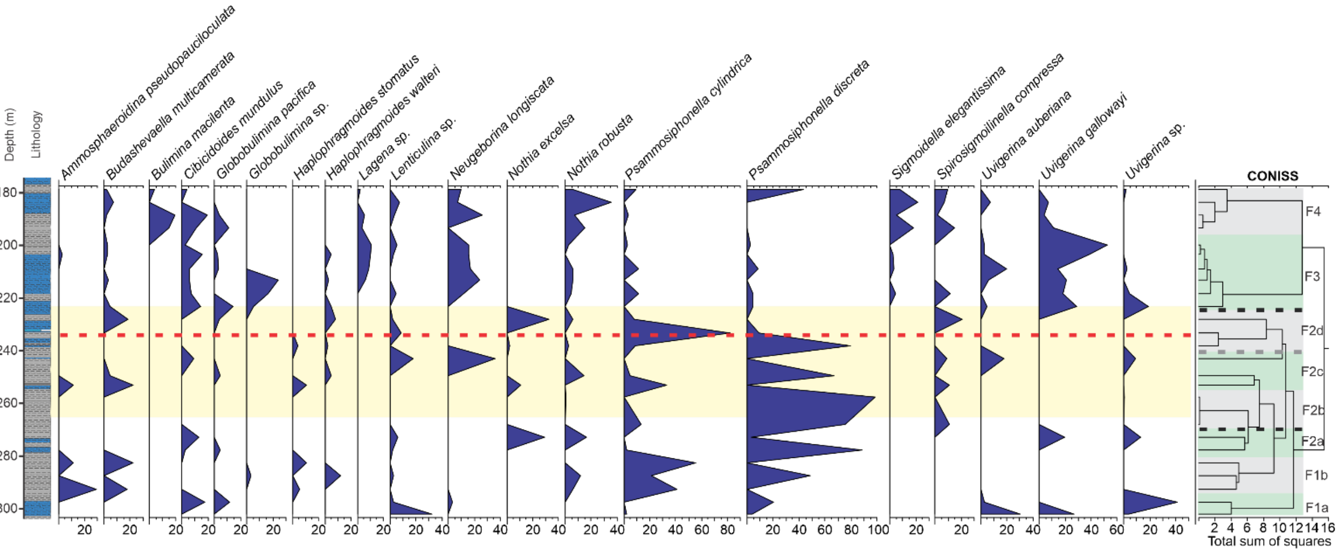

Figure S4. Distribution of the main benthic foraminiferal taxa (>5% relative abundance) across the upper Eocene–lower Oligocene interval in core ANH-SJ-1. The yellow shaded band represents the EOT, and the red dashed line marks the position of the EOB, as constrained by the age model developed in this study. The dendrogram on the right displays the results of the CONISS cluster analysis, which defines stratigraphically constrained assemblage groups (F1a–F4). The transition from F2a to F2b closely aligns with the onset of the EOT, and the shift from F2d to F3 corresponds to its termination. The shaded gray and green bars represent potential ecological clusters, and the black dashed lines highlight transitions that coincide with the Pre-EOT, EOT, and Post-EOT intervals. This ecological zonation provides independent support for the stratigraphic framework used in this study.

Table S7. Summary of PCA results in terms of eigenvalue and % variance for elements measured by XRF.

PC	Eigenvalue	% Variance	Cumulative %
1	0.563	61	61
2	0.12	13	74
3	0.00713	7.7	81.7
4	0.0461	5	86.7
5	0.0363	3.9	90.7
6	0.0247	2.7	93.3
7	0.02	2.2	95.5
8	0.0151	1.6	97.1
9	0.0109	1.2	98.3
10	0.00589	0.64	99
11	0.000316	0.34	99.3
12	0.00249	0.27	99.6
13	0.00142	0.15	99.7
14	0.00119	0.13	99.9
15	9.21E-06	0.1	100
16	0.000329	0.04	100

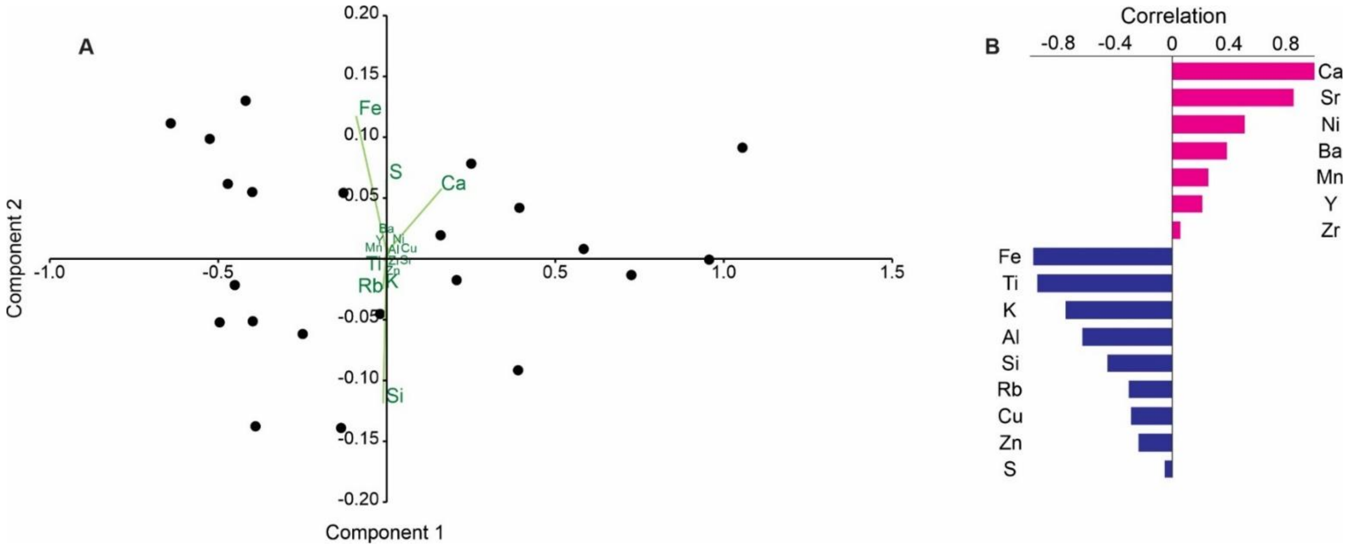

Figure S5. A. Principal Component Analysis (PCA) of elements measured by XRF in sediment samples showing element loadings in the first two principal components (Component 1 and Component 2). In the biplot graph, elements associated with biogenic sources (Ca, Sr) exhibit positive loadings in the first component, indicating their association with marine or biogenic material, possibly related to carbonates of marine origin. On the other hand, elements typical of terrigenous sources (Fe, Ti, K, Al) exhibit negative charges, suggesting a contribution from materials of continental origin, primarily silicate and clay minerals associated with erosive processes. The correlation bar chart on the right illustrates the strength and direction of the correlations between each element and the first two principal components, providing insight into the sources and compatibilities of the elements in the analyzed samples.

Table S8. Elements measured by XRF for the ANH-SJ-1 drill core samples.

SAMPLE ID	Ca	Sr	Ni	Ba	Mn	Y	Zr	Fe	Ti	K	Al	Si	Rb	Cu	Zn	S
SJ-974.8-BIO	1.66	0.27	0.04	0.10	0.02	0.01	0.05	1.93	0.16	0.27	0.13	1.20	0.04	0.01	0.03	0.27
SJ-1006.5-BIO	1.13	0.19	0.04	0.06	0.01	0.01	0.05	2.12	0.18	0.30	0.14	1.30	0.04	0.01	0.03	0.31
SJ-1025.2-BIO	1.19	0.18	0.03	0.09	0.02	0.01	0.05	2.22	0.19	0.31	0.16	1.26	0.04	0.01	0.03	0.41
SJ-1053.5-BIO	1.05	0.15	0.04	0.06	0.02	0.01	0.05	2.34	0.20	0.34	0.17	1.31	0.04	0.01	0.03	0.24
SJ-1075.5-BIO	1.36	0.20	0.04	0.10	0.02	0.01	0.06	2.14	0.19	0.32	0.16	1.22	0.04	0.01	0.03	0.23
SJ-1100.8-BIO	0.83	0.12	0.03	0.04	0.02	0.01	0.05	2.41	0.21	0.38	0.17	1.27	0.04	0.01	0.03	0.15
SJ-1125.8-BIO	1.50	0.20	0.03	0.09	0.02	0.01	0.05	2.09	0.19	0.35	0.17	1.25	0.04	0.02	0.03	0.21
SJ-1150.5-BIO	0.70	0.14	0.03	0.06	0.02	0.01	0.05	2.40	0.23	0.38	0.19	1.40	0.04	0.02	0.03	0.26
SJ-1175.5-BIO	0.49	0.12	0.03	0.09	0.02	0.01	0.06	2.57	0.23	0.39	0.18	1.34	0.04	0.02	0.05	0.28
SJ-1200.5-BIO	0.42	0.09	0.03	0.03	0.02	0.01	0.04	2.56	0.23	0.38	0.16	1.26	0.03	0.01	0.03	0.28
SJ-1225.6-BIO	1.01	0.15	0.03	0.09	0.02	0.02	0.06	2.37	0.20	0.36	0.17	1.27	0.04	0.01	0.03	0.26
SJ-1258.2-BIO	0.40	0.09	0.03	0.05	0.02	0.01	0.04	2.69	0.23	0.37	0.16	1.18	0.04	0.01	0.03	0.26
SJ-1275.5-BIO	0.46	0.12	0.03	0.08	0.02	0.01	0.06	2.68	0.23	0.37	0.18	1.27	0.05	0.02	0.03	0.30
SJ-1299.4-BIO	0.50	0.12	0.03	0.06	0.02	0.01	0.06	2.56	0.23	0.42	0.19	1.40	0.05	0.01	0.04	0.16
SJ-1325.1-BIO	0.41	0.13	0.03	0.08	0.02	0.01	0.05	2.63	0.23	0.40	0.18	1.34	0.05	0.01	0.03	0.24
SJ-1350.7-BIO	0.60	0.12	0.03	0.05	0.02	0.01	0.05	2.46	0.22	0.40	0.19	1.32	0.05	0.01	0.03	0.32
SJ-1375.5-BIO	1.80	0.16	0.03	0.08	0.03	0.02	0.05	1.96	0.17	0.32	0.16	1.13	0.04	0.01	0.03	0.25
SJ-1400.1-BIO	0.51	0.12	0.03	0.04	0.01	0.01	0.04	2.62	0.22	0.38	0.18	1.25	0.04	0.01	0.03	0.31
SJ-1425.5-BIO	0.53	0.12	0.03	0.09	0.01	0.02	0.05	2.70	0.22	0.37	0.19	1.24	0.05	0.02	0.03	0.35
SJ-1450.5-BIO	0.35	0.11	0.03	0.06	0.02	0.01	0.05	2.83	0.23	0.39	0.19	1.26	0.04	0.02	0.03	0.26
SJ-1475.2-BIO	0.74	0.16	0.03	0.07	0.01	0.01	0.04	2.49	0.20	0.30	0.18	1.26	0.04	0.02	0.03	0.33
SJ-1500.5-BIO	1.09	0.17	0.03	0.02	0.01	0.01	0.03	2.34	0.19	0.28	0.19	1.23	0.03	0.01	0.03	0.31

Table S9. Statistical analysis of micropaleontological indices using Shapiro-Wilk and Kruskal-Wallis Tests for upper Eocene and lower Oligocene. CN: Calcareous nannofossils, BF: Benthic foraminifera, Pal: Palynology.

Variable	Shapiro-Wilk upper Eocene _p	Shapiro-Wilk lower Oligocene_p	Kruskal-Wallis _p
Abundance CN	0.025	0.933	0.000
Dominance D CN	0.130	0.888	0.001
Shannon H' CN	0.010	0.054	0.065
Chao-1 CN	0.269	0.278	0.000
% Cold CN	0.000	0.000	0.407
% Temperate CN	0.002	0.393	0.897
% Warm CN	0.129	0.253	0.113
I°T_ CN	0.490	0.292	0.192
% Eutrophic CN	0.152	0.957	0.046
% Mesotrophic CN	0.345	0.954	0.659
% Oligotrophic CN	0.369	0.001	0.377
Iτ CN	0.444	0.962	0.111
Abundance BF	0.001	0.233	0.043
Dominance D BF	0.189	0.165	0.003
Shannon H' BF	0.271	0.885	0.002
Chao-1 BF	0.226	0.755	0.005
% Agglutinated BF	0.000	0.010	0.016
% Calcareous BF	0.000	0.010	0.015
Ratio Agg-Cal BF	0.000	0.010	0.015
% Epifaunal BF	0.006	0.024	0.002
% Infauna BF	0.006	0.024	0.002
% Dysoxic BF	0.593	0.619	0.073
% Oxic BF	0.183	0.137	0.021
% Suboxic BF	0.000	0.357	0.004
EBFOI BF	0.001	0.251	0.027
[O2] estimation BF	0.448	0.010	0.024
Abundance Pal	0.036	0.001	0.628
Dominance Pal	0.573	0.035	0.125
Shannon H' Pal	0.441	0.009	0.897
Chao-1 Pal	0.026	0.128	0.938
% Algae Pal	1.000	0.310	0.035
% Scolecodonts Pal	0.983	1.000	0.392
% Dinoflagelate Pal	0.026	0.000	0.600
% Spores Pal	0.109	0.321	0.586
% Foraminiferal Organic Linings Pal	0.001	0.010	0.045
% Fungi Pal	0.876	0.378	0.974
% Pollen Pal	0.788	0.259	0.035
T/M Pal	0.023	0.059	0.058
Palma Pal	0.043	0.308	0.218
Tree Pal	0.001	0.472	0.973
Mangrove Pal	0.000	0.396	0.077
Dinoflag Species richness (no range through) Pal	0.065	0.003	0.451

Table S10. T-test results of XRF ratios between upper Eocene and lower Oligocene.

Variable	t-Statistic	p-Value
Zr/Rb	-1.90	0.07
Zr/Al	-3.00	0.01
Sr/Al	-2.65	0.03
Mn/Fe	-0.47	0.64
Ca/Fe	-2.4	0.023
Fe/Ca	3.31	0.004
Ti/Ca	3.07	0.006
Ba/Al	-2.25	0.04
Ba/Ti	-2.11	0.05
Ca/Ti	-2.24	0.04
Ca/Al	-2.54	0.022
Sr/Ca	2.43	0.025
Ti/Al	0.02	0.98
Rb/Sr	2.47	0.02
Si/Al	-3.11	0.01
Zn/Al	-1.411	0.19
Cu/Al	-1.761	0.09
Rb/Al	-2.32	0.03
Al/Ti	0.17	0.87
K/Al	-0.30	0.7
K/Rb	2.27	0.03
Ba/Sr	0.57	0.57

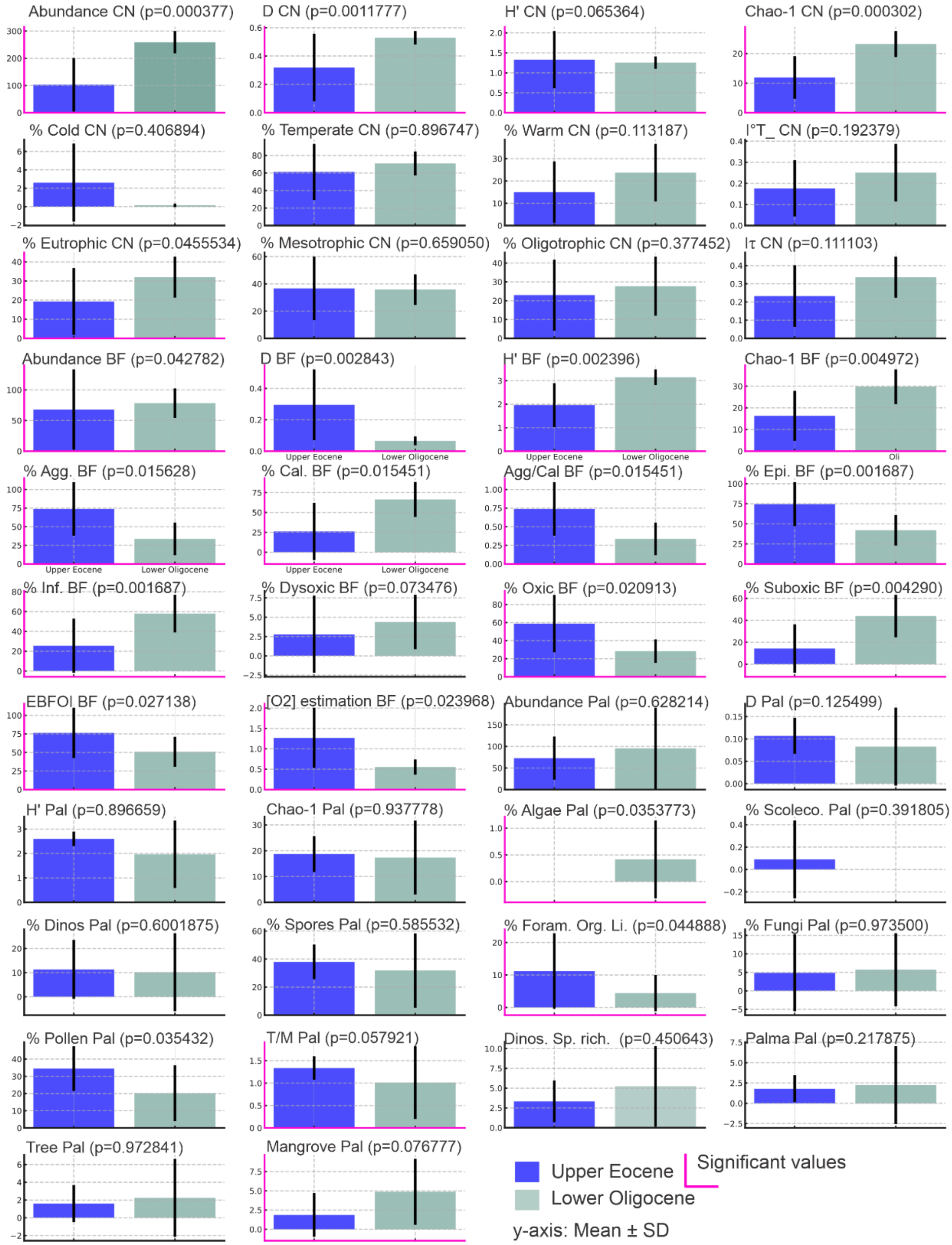

Figure S6. Statistical comparison of ecological and environmental proxies between the upper Eocene and lower Oligocene in the ANH-SJ-1 drill core. Bars represent the mean ± standard deviation (SD) for each variable. Significant differences are shown in green, while non-significant results are in black.

Table S11. Statistical analysis of micropaleontological indices using ANOVA and T-tests for pre-EOT, EOT, and post-EOT Intervals. CN: Calcareous nannofossils, BF: Benthic foraminifera, Pal: Palynology.

Variable	ANOVA_p	T-Test PreEOT_vs_EOT p	T-Test EOT_vs_Post_EOT_p	T-Test Pre_EOT_vs_Post_EOT_p
Abundance CN	0.000	0.191	0.466	0.893
Dominance D CN	0.051	0.567	0.436	0.009
Shannon H' CN	0.217	0.180	0.314	0.382
Chao-1 CN	0.000	0.537	0.181	0.127
% Cold CN	0.064	0.037	0.690	0.039
% Temperate CN	0.809	0.963	0.733	0.493
% Warm CN	0.128	0.275	0.023	0.155
I°T_ CN	0.236	0.426	0.039	0.185
% Eutrophic CN	0.075	0.348	0.773	0.018
% Mesotrophic CN	0.831	0.686	0.912	0.592
% Oligotrophic CN	0.167	0.029	0.013	0.758
Iτ CN	0.030	0.015	0.319	0.032
Abundance BF	0.742	0.433	0.201	0.871
Dominance D BF	0.022	0.900	0.181	0.006
Shannon H' BF	0.004	0.947	0.133	0.001
Chao-1 BF	0.010	0.812	0.045	0.005
% Agglutinated BF	0.003	0.853	0.104	0.001
% Calcareous BF	0.003	0.853	0.104	0.001
Ratio Agg-Cal BF	0.003	0.853	0.104	0.001
% Epifaunal BF	0.002	0.795	0.043	0.001
% Infauna BF	0.002	0.795	0.043	0.001
% Dysoxic BF	0.266	0.472	0.815	0.105
% Oxic BF	0.017	0.895	0.135	0.005
% Suboxic BF	0.001	0.889	0.060	0.000
EBFOI BF	0.045	0.940	0.163	0.015
[O2] estimation BF	0.020	0.893	0.167	0.006
Abundance Pal	0.533	0.953	0.518	0.387
Dominance Pal	0.041	0.530	0.206	0.031
Shannon H' Pal	0.415	0.529	0.671	0.257
Chao-1 Pal	0.869	0.647	0.681	0.981
% Algae Pal	0.077		0.089	0.089
% Scolecodonts Pal	0.577	0.339		0.339
% Dinoflagelate Pal	0.609	0.118	0.424	0.660
% Spores Pal	0.097	0.097	0.038	0.336
% Foraminiferal Organic Linings Pal	0.156	0.096	0.973	0.083
% Fungi Pal	0.858	0.758	0.998	0.603
% Pollen Pal	0.119	0.754	0.206	0.059
T/M Pal	0.281	0.004	0.697	0.195
Palma Pal	0.784	0.496	0.534	0.722
Tree Pal	0.740	0.820	0.555	0.609
Mangrove Pal	0.095	0.431	0.241	0.081
Dinoflag Species richness (no range through) Pal	0.257	0.148	0.123	0.372

Table S12. ANOVA summary of XRF ratios pre-EOT, EOT, and post-EOT Intervals.

Variable	Pre-EOT Mean	Pre-EOT SD	EOT Mean	EOT SD	Post-EOT Mean	Post-EOT SD	p-Value
Zr/Rb	1.136	0.054	1.227	0.111	1.136	0.054	1.227
Zr/Al	0.247	0.049	0.301	0.029	0.247	0.049	0.301
Sr/Al	0.763	0.185	0.661	0.111	0.763	0.185	0.661
Ca/Fe	0.348	0.273	0.218	0.095	0.348	0.273	0.218
Fe/Ca	4.149	2.300	5.154	1.526	4.149	2.300	5.154
Ti/Ca	0.349	0.191	0.455	0.127	0.349	0.191	0.455
Ca/Ti	4.114	3.470	2.456	1.081	4.114	3.470	2.456
Ca/Al	4.581	3.264	3.101	1.223	4.581	3.264	3.101
Sr/Ca	0.204	0.067	0.226	0.047	0.204	0.067	0.226
Rb/Sr	0.302	0.095	0.379	0.054	0.302	0.095	0.379
Si/Al	6.851	0.258	7.390	0.256	6.851	0.258	7.390

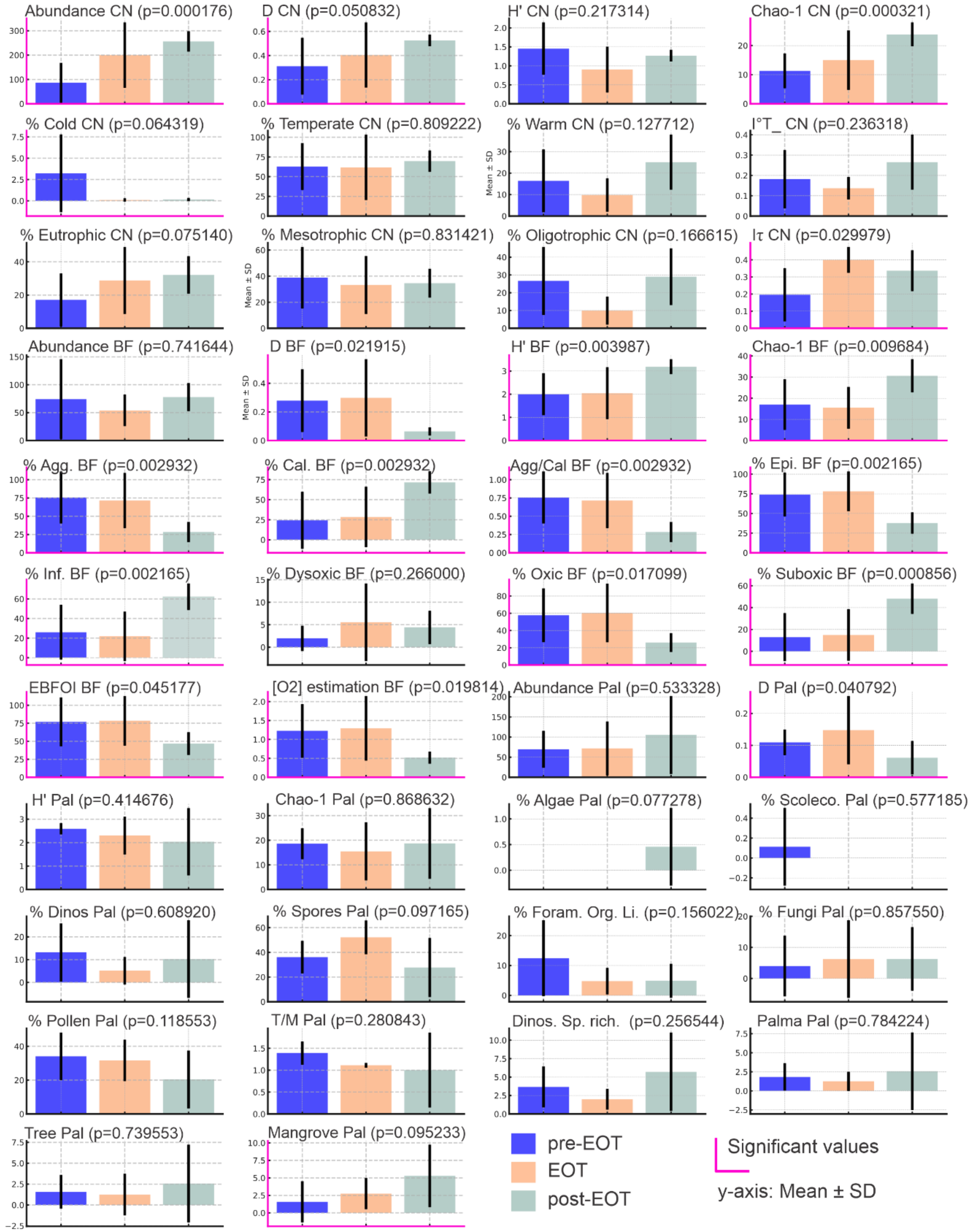

Figure S7. Statistical comparison of ecological and environmental proxies between pre-EOT, EOT, and post-EOT intervals.

Table S13. Summary by depth of maximum likelihood age (MLA) estimates for drill core ANH-SJ-1. The table includes Q25 (25th percentile) and Q75 (75th percentile) values, along with their corresponding graphical representations. † Depths associated with the EOT based on calcareous nannofossils bioevents. ‡ Depth intervals that encompass the EOT. § Depths with the highest MLA estimates are considered more reliable for age interpretation.

Depth	MLA	Q_25	Q_75	Number in graph
183.5	32.208	27.850	71.180	1
193.3	32.554	19.787	42.613	2
199.6	23.249	20.052	38.296	3
203.3	32.045	21.050	57.578	4
208.9	23.249	17.425	39.355	5
213.2	23.493	20.826	43.814	6
223.2	16.041	24.043	75.761	7
228.1	32.248§	27.239§	43.936§	8
233.1	32.147	23.778	66.639	9
238.0†	32.248§	27.708§	39.090§	10
243.0‡	32.228§	28.420§	42.226§	11
249.5‡	32.839§	28.013§	44.323§	12
252.9†	32.208	27.708	73.012	13
257.6†	23.249	20.744	41.045	14
262.7†	32.289	25.549	75.721	15
267.8	25.407	23.350	70.386	16
272.7	21.864	17.242	58.474	17
277.6	17.975	15.145	41.818	18
282.6	31.902	25.102	74.438	19
287.6	13.821	14.636	50.452	20
292.5	31.882	21.660	54.056	21
297.5	32.696	23.106	43.570	22
302.2	32.961	25.244	75.415	23

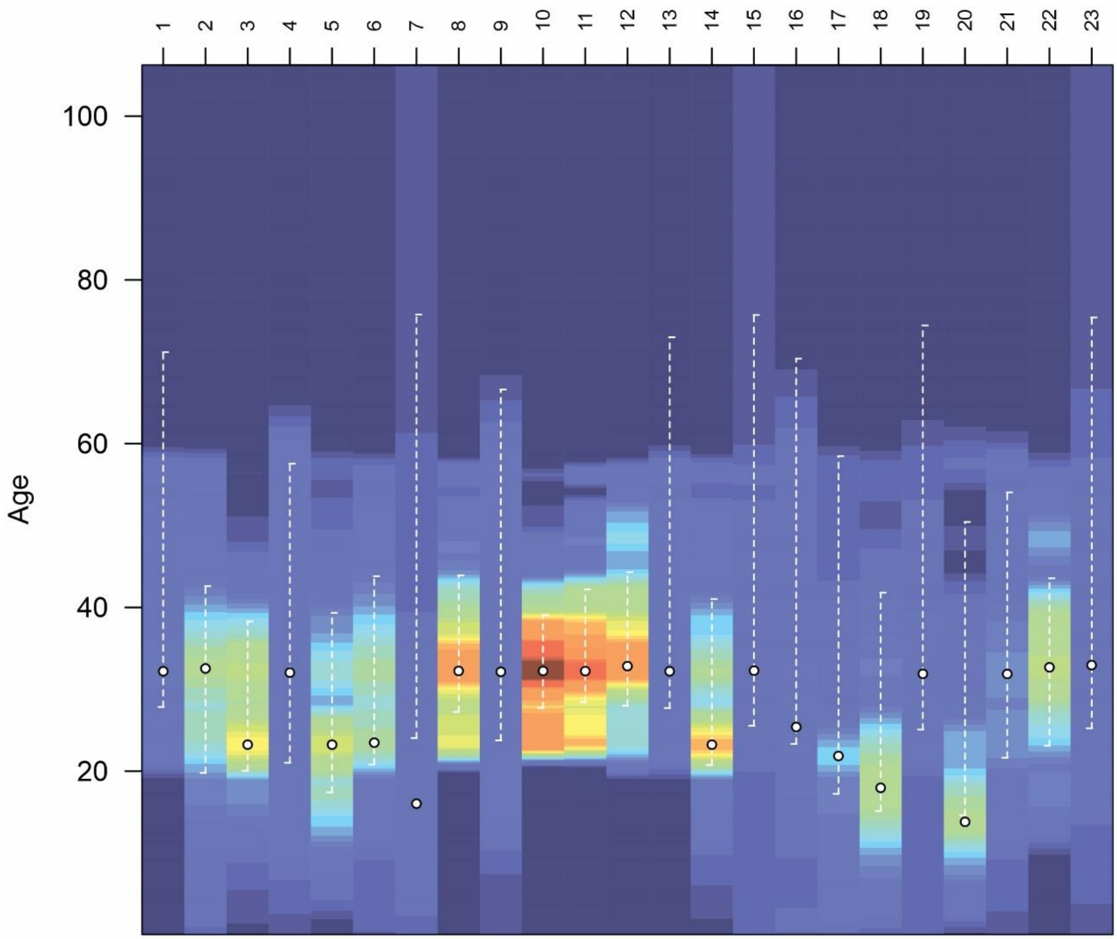

Figure S8. Maximum likelihood age (circles) for the ANH-SJ-1 samples. Vertical dashed lines denote confidence intervals.

Table S14. Calculated ages for the samples analyzed in this study, including their corresponding depths and associated confidence intervals.

ID Sample	Corrected depth in m according to Arias-Villegas et al. (2023)	Calculated age in this work	Confidence interval
SJ-900.8-BIO	178.6	32.2	±0.4
SJ-925.5-BIO	183.5	32.4	±0.3
SJ-950.5-BIO	188.5	32.5	±0.3
SJ-974.8-BIO	193.3	32.7	±0.3
SJ-1006.5-BIO	199.6	32.9	±0.3
SJ-1025.2-BIO	203.3	33.0	±0.3
SJ-1053.5-BIO	208.9	33.1	±0.2
SJ-1075.5-BIO	213.2	33.3	±0.2
SJ-1100.8-BIO	218.3	33.4	±0.2
SJ-1125.8-BIO	223.2	33.6	±0.2
SJ-1150.5-BIO	228.1	33.7	±0.2
SJ-1175.5-BIO	233.1	33.9	±0.2
SJ-1200.5-BIO	238.0	34.0	±0.2
SJ-1225.6-BIO	243.0	34.2	±0.2
SJ-1258.2-BIO	249.5	34.4	±0.2
SJ-1275.5-BIO	252.9	34.5	±0.2
SJ-1299.4-BIO	257.6	34.6	±0.3
SJ-1325.1-BIO	262.7	34.8	±0.3
SJ-1350.7-BIO	267.8	34.9	±0.3
SJ-1375.5-BIO	272.7	35.1	±0.3
SJ-1400.1-BIO	277.6	35.2	±0.4
SJ-1425.5-BIO	282.6	35.4	±0.4
SJ-1450.5-BIO	287.6	35.5	±0.4
SJ-1475.2-BIO	292.5	35.7	±0.4
SJ-1500.5-BIO	297.5	35.8	±0.4
SJ-1523.9-BIO	302.2	36.0	±0.5

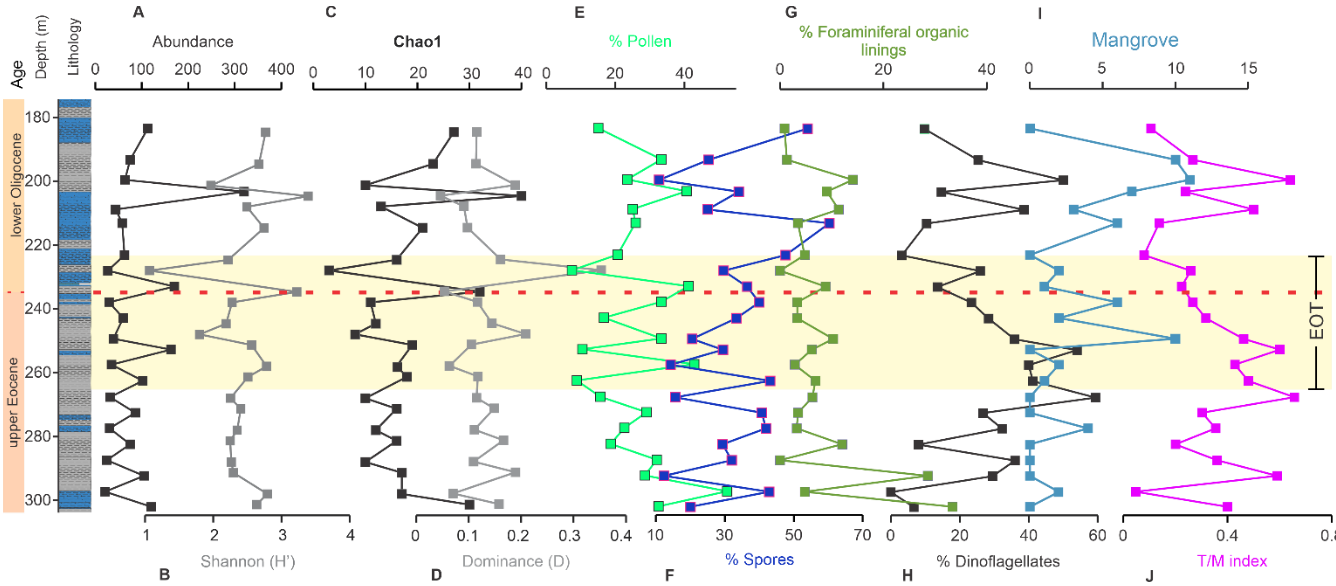

Figure S9. Temporal and depth evolution of various palynological parameters in the ANH-SJ-1 drill core. The vertical axis represents time in millions of years (Ma) and core lithology (depth in meters). Panel (A) shows the absolute abundance of palynomorphs (total counts), while panels (B) and (C) illustrate the H' (Shannon) and Chao1 diversity indices. Panel (D) shows the dominance index (D), and panels (E), (F), (G), (H), and (I) show the relative abundances of pollen, spores, foraminiferal organic linings, dinoflagellates, and mangrove, respectively. Finally, panel (J) presents the T/M index. Colored indices and relative abundances (e.g., % pollen, %spores, % foraminiferal organic linings, mangrove, T/M index) are those that fall within or near statistical significance thresholds in the Kruskal-Wallis (K-W) and ANOVA tests. The red dashed line indicates the EOB.

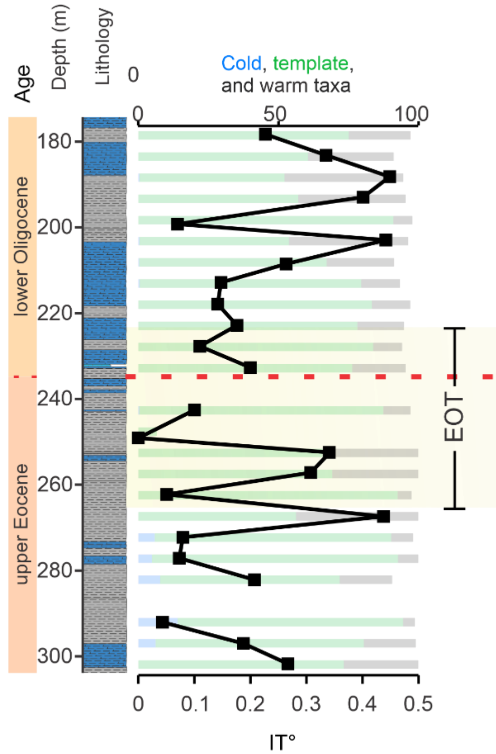

Figure S10. Temporal and stratigraphic evolution of the IT° index along the ANH-SJ-1 drill core. This index did not show statistically significant differences based on Kruskal–Wallis (K-W) and ANOVA tests. The red dashed line indicates the position of the EOB.

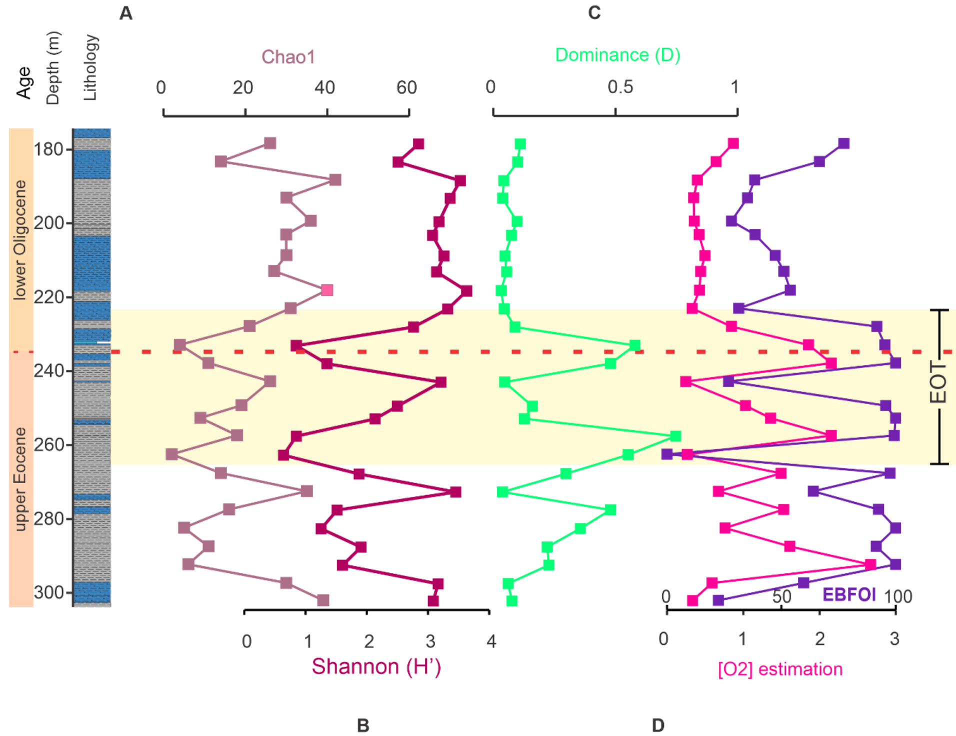

Figure S11. Temporal and depth evolution of indices measured in planktonic and benthic foraminiferal assemblages in the ANH-SJ-1 drill core. The vertical axis represents time (Ma) along with the core lithology (depth in meters). Panels (A) and (B) present the Chao1, H' (Shannon) diversity indices for benthic foraminifera, and panel (C) depicts the dominance index (D). Panel (D) shows oxygenation estimates ([O_2]), along with the EBFOI measurement. The red dashed line indicates the EOB.

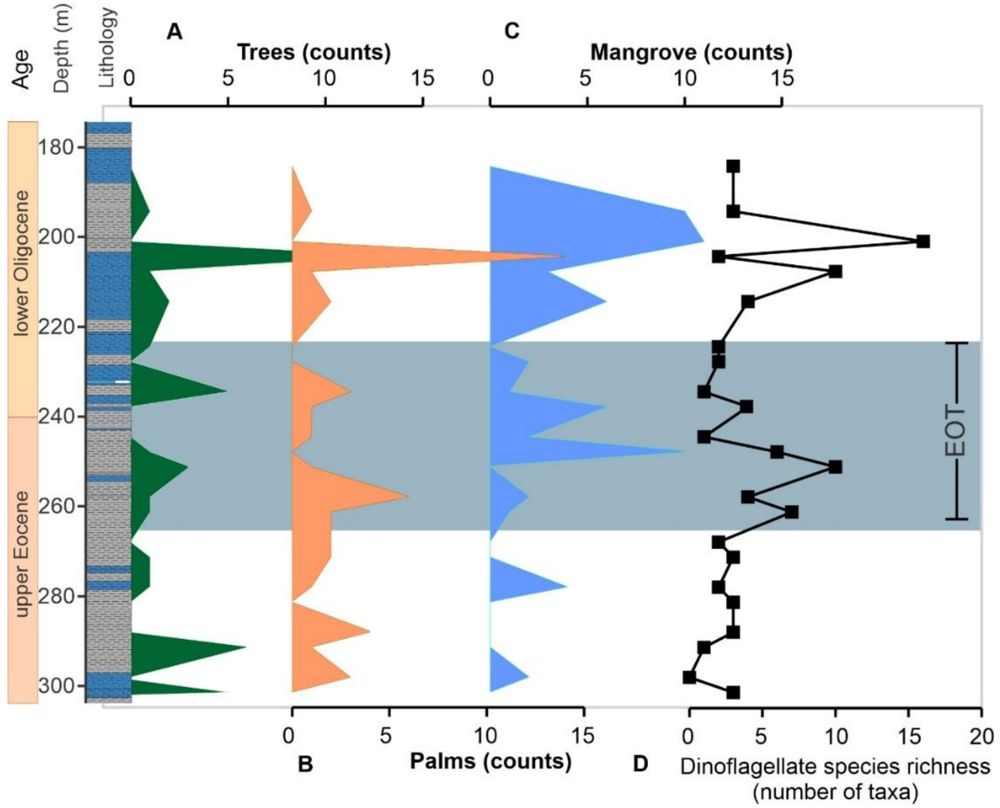

Figure S12. Temporal evolution of terrestrial palynological components and dinoflagellate species richness in the upper Eocene–lower Oligocene interval of the ANH-SJ-1. A. Relative abundance of tree pollen. B. Palm pollen. C. Mangrove pollen. D. Species richness of dinoflagellate cyst.

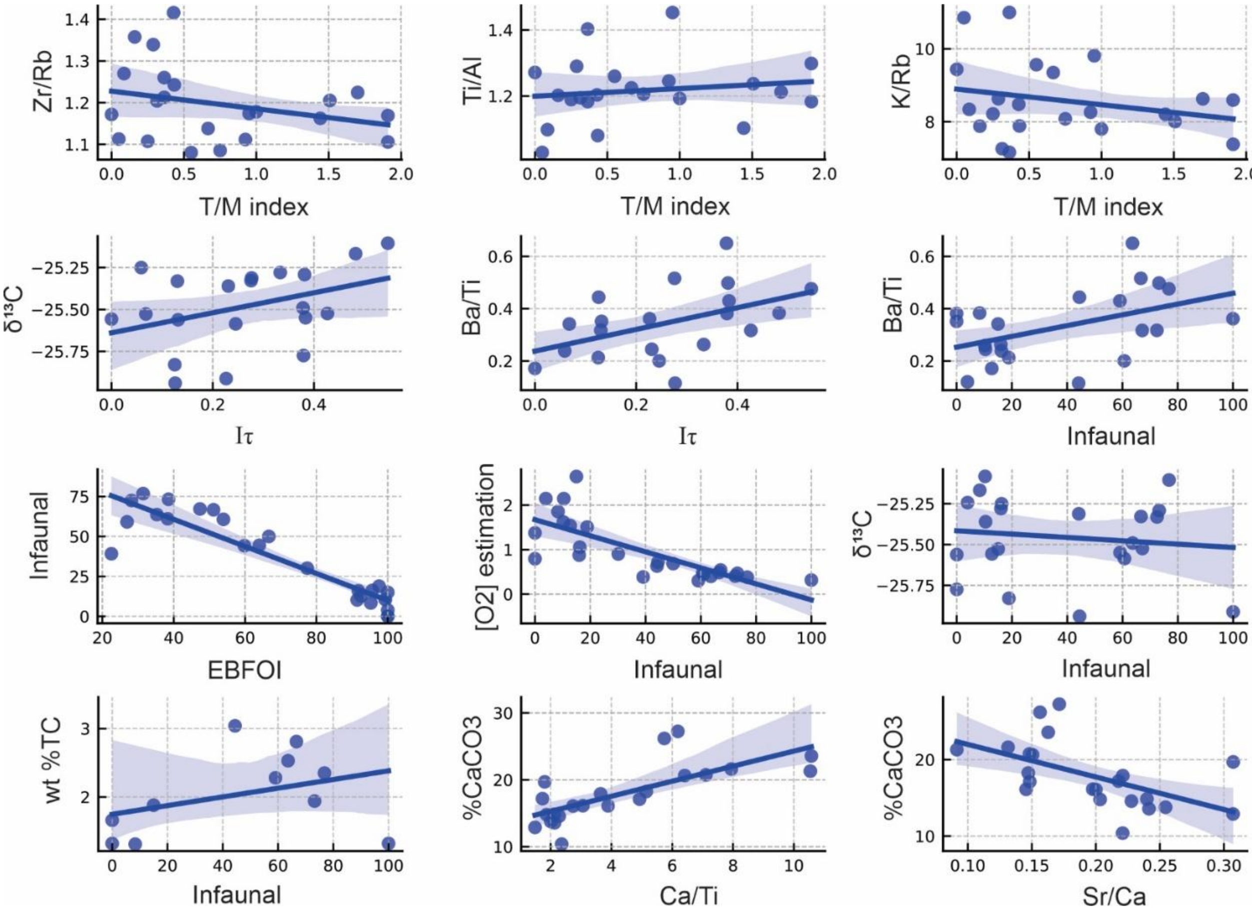

Figure S13. Correlations between sedimentary and biotic proxies: The T/M index exhibits associations with terrigenous proxies (Zr/Rb, Ti/Al, K/Rb). Proportions of benthic infauna (Infaunal) and calcareous nannofossils (Itro) are related to productivity proxies (Ba/Ti, %CaCO3) and oxygenation indicators (EBFOI, [O2] estimation). Regression lines show trends with 95% confidence intervals.

References

Agnini, C., Fornaciari, E., Rio, D., Tateo, F., Backman, J., and Giusberti, L.: Responses of calcareous nannofossil assemblages, mineralogy and geochemistry to the environmental perturbations across the Paleocene/Eocene boundary in the Venetian Pre-Alps, Mar Micropaleontol, 63, 19–38, https://doi.org/10.1016/j.marmicro.2006.10.002, 2007.

Arias-Villegas, V., Bedoya Agudelo, E. L., Vallejo-Hincapié, F., Aubry, M.-P., and Pardo-Trujillo, A.: Late Eocene to Early Miocene calcareous nannofossil biostratigraphy from the ANH-San Jacinto- 1 well: Stratigraphic implications for the Sinú-San Jacinto basin in the Caribbean region of Colombia, J South Am Earth Sci, 128, 104470, https://doi.org/10.1016/j.jsames.2023.104470, 2023.

Aubry, M.-P.: Late Paleogene Calcareous Nannoplankton Evolution: A Tale of Climatic Deterioration, in: Eocene-Oligocene Climatic and Biotic Evolution, edited by: Prothero, D. R. and Berggren, W. A., Princeton University Press, Princeton, NJ, 272–309, https://doi.org/10.1515/9781400862924.272, 1992.

Bukry, D.: Low-Latitude Coccolith Biostratigraphic Zonation, in: Initial Reports of the Deep Sea Drilling Project, 15, U.S. Government Printing Office, 685–703, https://doi.org/10.2973/dsdp.proc.15.116.1973, 1973.

Cao, W., Yang, Q., Ji, F., and Liu, C.: Influence of N, P, and Fe availability on Braarudosphaera bigelowii, Trichodesmium, Crocosphaera, and noncyanobacterial diazotrophs: a review, Front Mar Sci, 11, https://doi.org/10.3389/fmars.2024.1467599, 2024.

Cappelli, C., Bown, P. R., Westerhold, T., Bohaty, S. M., de Riu, M., Lobba, V., Yamamoto, Y., and Agnini, C.: The Early to Middle Eocene Transition: An Integrated Calcareous Nannofossil and Stable Isotope Record From the Northwest Atlantic Ocean (Integrated Ocean Drilling Program Site U1410), Paleoceanogr Paleoclimatol, 34, 1913–1930, https://doi.org/10.1029/2019PA003686, 2019.

Hutchinson, D. K., Coxall, H. K., Lunt, D. J., Steinthorsdottir, M., de Boer, A. M., Baatsen, M., von der Heydt, A., Huber, M., Kennedy-Asser, A. T., Kunzmann, L., Ladant, J.-B., Lear, C. H., Moraweck, K., Pearson, P. N., Piga, E., Pound, M. J., Salzmann, U., Scher, H. D., Sijp, W. P., Śliwińska, K. K., Wilson, P. A., and Zhang, Z.: The Eocene–Oligocene transition: a review of marine and terrestrial proxy data, models and model–data comparisons, Climate of the Past, 17, 269–315, https://doi.org/10.5194/cp-17-269-2021, 2021.

Monechi, S., Buccianti, A., and Gardin, S.: Biotic signals from nannoflora across the iridium anomaly in the upper Eocene of the Massignano section: evidence from statistical analysis, Mar Micropaleontol, 39, 219–237, https://doi.org/10.1016/S0377-8398(00)00022-0, 2000.

Newsam, C., Bown, P. R., Wade, B. S., and Jones, H. L.: Muted calcareous nannoplankton response at the Middle/Late Eocene Turnover event in the western North Atlantic Ocean, Newsl Stratigr, 50, 297–309, https://doi.org/10.1127/nos/2016/0306, 2017.

Persico, D. and Villa, G.: Eocene–Oligocene calcareous nannofossils from Maud Rise and Kerguelen Plateau (Antarctica): paleoecological and paleoceanographic implications, Mar Micropaleontol, 52, 153–179, https://doi.org/10.1016/j.marmicro.2004.05.002, 2004.

Siesser, W. G., Bralower, T. J., and De Carlo, E. H.: Mid-Tertiary Braarudosphaera-Rich Sediments on the Exmouth Plateau, in: Proceedings of the Ocean Drilling Program, 122 Scientific Results, Ocean Drilling Program, https://doi.org/10.2973/odp.proc.sr.122.163.1992, 1992.

Tremolada, F. and Bralower, T. J.: Nannofossil assemblage fluctuations during the Paleocene–Eocene Thermal Maximum at Sites 213 (Indian Ocean) and 401 (North Atlantic Ocean): palaeoceanographic implications, Mar Micropaleontol, 52, 107–116, https://doi.org/10.1016/j.marmicro.2004.04.002, 2004.

Vieyra-Mexicano, C., Souza, V., and Pajares, S.: Distribution of the N2-fixing cyanobacterium Candidatus Atelocyanobacterium thalassa in the Mexican Pacific upwelling system under two contrasting El Niño Southern Oscillation conditions, Environ Microbiol Rep, 16, https://doi.org/10.1111/1758-2229.13237, 2024.

Villa, G., Fioroni, C., Pea, L., Bohaty, S., and Persico, D.: Middle Eocene–late Oligocene climate variability: Calcareous nannofossil response at Kerguelen Plateau, Site 748, Mar Micropaleontol, 69, 173–192, https://doi.org/10.1016/j.marmicro.2008.07.006, 2008.

Villa, G., Fioroni, C., Persico, D., Roberts, A. P., and Florindo, F.: Middle Eocene to Late Oligocene Antarctic glaciation/deglaciation and Southern Ocean productivity, Paleoceanography, 29, 223–237, https://doi.org/10.1002/2013PA002518, 2014.

Wei, W. and Wise, S. W.: Biogeographic gradients of middle Eocene-Oligocene calcareous nannoplankton in the South Atlantic Ocean, Palaeogeogr Palaeoclimatol Palaeoecol, 79, 29–61, https://doi.org/10.1016/0031-0182(90)90104-F, 1990.

Westerhold, T., Marwan, N., Drury, A. J., Liebrand, D., Agnini, C., Anagnostou, E., Barnet, J. S. K., Bohaty, S. M., De Vleeschouwer, D., Florindo, F., Frederichs, T., Hodell, D. A., Holbourn, A. E., Kroon, D., Lauretano, V., Littler, K., Lourens, L. J., Lyle, M., Pälike, H., Röhl, U., Tian, J., Wilkens, R. H., Wilson, P. A., and Zachos, J. C.: An astronomically dated record of Earth's climate and its predictability over the last 66 million years, Science (1979), 369, 1383–1387, https://doi.org/10.1126/science.aba6853, 2020.

Ziveri, P., Thunell, R. C., and Rio, D.: Export production of coccolithophores in an upwelling region: Results from San Pedro Basin, Southern California Borderlands, Mar Micropaleontol, 24, 335–358, https://doi.org/10.1016/0377-8398(94)00017-H, 1995.

Ziveri, P., Baumann, K.-H., Böckel, B., Bollmann, J., and Young, J. R.: Biogeography of selected Holocene coccoliths in the Atlantic Ocean, in: Coccolithophores, edited by: Thiertein, H. R. and Young, J. R., Springer Berlin Heidelberg, Berlin, Heidelberg, 403–428, https://doi.org/10.1007/978-3-662-06278-4_15, 2004.